Effects of dimerization on protein electron transfer

Amsterdam, M.C. van; Ubbink, M.; Jeuken, L.J.C.; Verbeet, M.P.; Canters, G.W.; Messerschmidt, A.

FULL PAPER

Effects of Dimerization on Protein Electron Transfer

Irene M. C. van Amsterdam,[a] Marcellus Ubbink,[a] Lars J. C. Jeuken,[a] Martin Ph. Verbeet,[a] Oliver Einsle,[b] Albrecht Messerschmidt,[b] and Gerard W. Canters*[a]

Abstract: In order to investigate the relationship between the rate of protein–protein electron transfer and the structure of the association complex, a dimer of the blue copper protein azurin was constructed and its electron exchange properties were determined. For this purpose, a site for covalent cross-linking was engineered by replacing the surface-exposed asparagine 42 with a cysteine. This mutation enabled the formation of disulfide-linked homodimers of azurin. Based on NMR line-broadening experiments, the electron self-exchange (e.s.e.) rate constant for this dimer was determined to be $4.2(\pm 0.7) \times 10^5 \, M^{-1}s^{-1}$, which is a sevenfold decrease relative to wild-type azurin. This difference is ascribed to a less accessible hydrophobic patch in the dimer. To discriminate between intramolecular electron transfer within a dimer and intermolecular electron transfer between two dimers, the e.s.e. rate constant of (Cu–Cu)-N42C dimers was compared with that of (Zn–Cu)- and (Ag–Cu)-N42C dimers. As Zn and Ag are redox inactive, the intramolecular electron transfer reaction in these latter dimers can be eliminated. The e.s.e. rate constants of the three dimers are the same and an upper limit for the intramolecular electron transfer rate of $10 \, s^{-1}$ could be determined. This rate is compatible with a Cu–Cu distance of 18 Å or more, which is larger than the Cu–Cu distance of 15 Å observed in the wild-type crystal structure that shows two monomers that face each other with opposing hydrophobic patches. Modelling of the dimer shows that the Cu–Cu distance should be in the range of $17 \, \text{Å} < r_{\text{Cu–Cu}} < 28 \, \text{Å}$, which is in agreement with the experimental findings. For efficient electron transfer, it appears crucial that the two molecules interact in the proper orientation. Direct cross-linking may disturb the formation of such an optimal electron transfer complex.

Keywords: azurin · copper · dimerization · electron transfer · NMR spectroscopy

Introduction

Many biological redox processes depend on protein-mediated electron transfer. In contrast to chemical reactions, which are strongly localized in space, electron transfers can take place over large distances (up to 20 Å) in the living cell. The importance of distance in controlling the rate of electron transfer in proteins is illustrated by the remarkable exponential relationship between rate and distance that covers about 12 orders of magnitude in the rate and about 20 Å in distance.[1] Besides distance, parameters such as thermodynamic driving force, reorganization energy, and donor–acceptor orientation also influence the rate of electron transfer. The Marcus theory[2] is often applied to analyze these parameters. Normally, a distance between two redox centers of less than ~20 Å will provide for electron tunneling that is sufficiently fast within a biological context.[1] Therefore, the redox centers that participate in inter-protein electron transfers have to be close to the edge of the protein; in general, they should be within 9 Å of the surface. On the other hand, the redox centers should be well protected by sufficient protein medium to prevent accidental aspecific electron exchange with exogenous redox partners. Within the reaction complex, the proteins should be oriented in such a way that the electron transfer rate is optimized.

Cross-linking has been used as a method to gain insight into the relative orientation of proteins in such short-lived complexes. Generally, cross-linking is achieved by using chemical reagents[3–16] such as 1-ethyl-3-[3-(dimethylamino)propyl]carbodiimide (EDC) or by engineered disulfide formation.[17, 18]

[a] Prof. Dr. G. W. Canters, I. M. C. van Amsterdam, Dr. M. Ubbink, Dr. L. J. C. Jeuken,[+] Dr. M. Ph. Verbeet
Leiden Institute of Chemistry
Gorlaeus Laboratories, Leiden University
P.O. Box 9502, 2300 RA Leiden (The Netherlands)
Fax: (+31) 71-5274349
E-mail: canters@chem.leidenuniv.nl

[b] Dr. O. Einsle, Dr. A. Messerschmidt
Max-Planck-Institut für Biochemie
Abteilung Strukturforschung
Am Klopferspitz 18a, 82152 Martinsried (Germany)

[+] Current address: Inorganic Chemistry Laboratory
South Parks Road, Oxford OX1 3QR (England)

Both methods produce so-called "zero-length" linkers, in which the proteins are directly linked without the introduction of connecting atoms. Often, it is found that the electron transfer rate decreases drastically by linking two proteins, which indicates that the complexes that are formed are not favourable for electron transfer; for example, in cross-linked complexes of cytochrome *f* and plastocyanin[14] and cytochrome *c* and cytochrome *c* peroxidase.[18] This observation is in agreement with the proposal that, in many cases, a rearrangement step is needed[7, 12, 19–23] after the formation of the association complex for electron transfer to occur. This means that, in the association complex in the first instance, the position and orientation of the partners with respect to each other is less productive for electron transfer. The first step must be followed, then, by rearrangement to a more "productive" orientation before electron transfer can occur. These observations suggest that fast electron transfer between proteins requires subtle and precise positioning and orientation of the two redox partners with respect to each other.

To better understand this phenomenon, we studied electron transfer in a well-defined cross-linked complex. For this purpose, a site for covalent cross-linking was engineered in azurin, a so-called blue copper protein that has been extensively characterized, structurally as well as mechanistically.[24–31] The 14 kD redox protein has a so-called type-1 copper site that is positioned about 7 Å beneath the protein surface and is coordinated by three strong ligands (N^{δ}-s of His117 and His46, and S^{γ} of Cys112) that are arranged in a planar configuration around the metal. Two weakly interacting groups (S^{δ} of Met121 and the carbonyl oxygen of Gly45) are located in axial positions. The copper ligand His117 is positioned in the middle of a hydrophobic patch, which is the surface area that is involved in electron transfer, including the electron self-exchange (e.s.e.) reaction.[29, 32–34] In the crystal structure of wild-type azurin, the hydrophobic patches of two azurin molecules face each other with a Cu–Cu distance of 15 Å (see Figure 1). The dimer packing shows two water molecules that connect the monomers by hydrogen bonds.[26, 27] Although no dimers are observed in solution, the very high e.s.e. rate constant ($\sim 10^6 \, \mathrm{M}^{-1}\mathrm{s}^{-1}$)[35–37] suggests that the association complex may have a similar structure in solution.[38] With the goal of obtaining a covalent azurin dimer in solution that resembles the non-covalent dimer in the crystal structure, a site for cross-linking was engineered at residue 42 (asparagine). With the introduction of a cysteine at this position, it was thought that it would be possible to form a disulfide bridge with retention of the orientation of the two azurin molecules with respect to each other (see Figure 1). The e.s.e. rate can then be used to monitor the influence of conformational flexibility around the Cys–Cys link on the intramolecular e.s.e. reaction. Formation of azurin dimers that followed this scheme was successful and the electron transfer characteristics could be studied in detail. In this way, we could determine an upper limit for the intramolecular electron transfer rate in the N42C dimer. The findings are discussed in terms of the structure of the dimer in solution.

Electron self-exchange rate: The electron transfer properties of azurin were studied by looking at the e.s.e. reaction, that is,
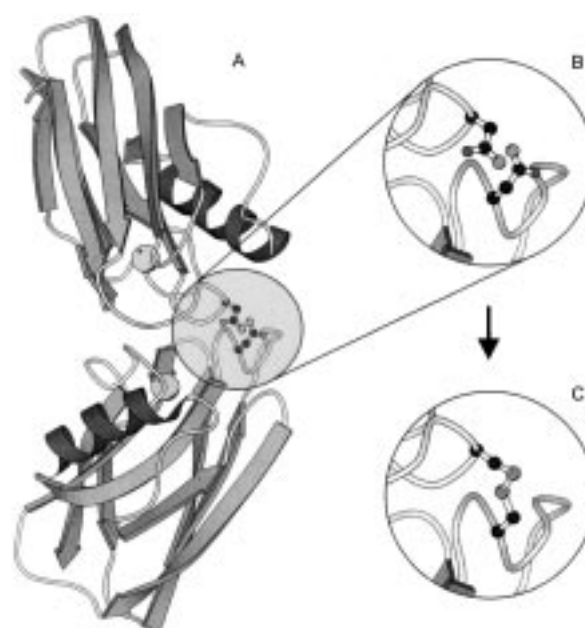

Figure 1. A) Two azurin molecules that face each other with opposing hydrophobic patches as observed in the crystal structure of azurin from *P. aeruginosa* (5azu.pdb).[26] The copper atoms are represented by spheres. B) Enlargement of region around position 42 that covers part of the interface between the two molecules. The heavy atoms of the asparagines at position 42 are in ball-and-stick representation. C) Asparagines 42 have been replaced by cysteines, which have been modelled to form a disulfide bond. The model is based on the crystal structure of wild-type azurin. Pictures are generated by MOLSCRIPT.[49]

the electron exchange reaction between identical redox partners [see Eq. (1)].

$$A_r + A_o \underset{k_{-1}}{\overset{k_1}{\rightleftharpoons}} A_o + A_r \qquad (1)$$

Here, A_r and A_o represent the reduced and oxidized partners, respectively. Although e.s.e. reactions may not be of physiological relevance in the case of azurin, theoretically they are of interest, because $\Delta G^0 = 0$, and $k_1 = k_{-1} \equiv k_{ese}$ (electron self-exchange rate constant), which simplifies the analysis of experimental data. The e.s.e. rate constant can be determined from the broadening of NMR signals of the nuclei that are close to the redox site when a small amount of oxidized (paramagnetic) azurin is introduced into a solution of the reduced protein. The broadening, ΔT_2^{-1}, is caused by the magnetic pulses that the protons experience during the brief periods when the azurin is paramagnetic as the result of an electron transfer event. As long as the "strong pulse" or "slow exchange" condition applies for the NMR experiments, k_{ese} can be obtained by using Equation (2):[37]

$$\Delta T_2^{-1} = k_{obs} = k_{ese} [A_o] \qquad (2)$$

In the case of a partly oxidized solution of covalent dimers, four different species can be distinguished: A_rA_r, A_rA_o, A_oA_r and A_oA_o. Since we shall be dealing with solutions in which the degree of oxidation is less than 8.5 %, the last species can be neglected for practical purposes. To analyze the effect of the electron exchange reaction on the NMR signals of the reduced species, we consider the fate of a particular monomer, which is denoted by an asterisk (A^*). From the point of view

of NMR line-broadening, A_r*A_o plus A_oA_r* and A_r*A_r represent populations with different kinetic characteristics. Under our experimental conditions, the signals from the diamagnetic species (A_r*) in the A_r*A_o plus A_oA_r* population represent less than 15% of the total signals from the A_r* species (the other 85% are derived from the A_r*A_r population). Therefore, the contribution of the A_r*A_o plus A_oA_r* population is negligible. The diamagnetic lifetime of A_r* in A_r*A_r depends on two processes, α and β, as depicted schematically in Figure 2 [Eq. (3)]:
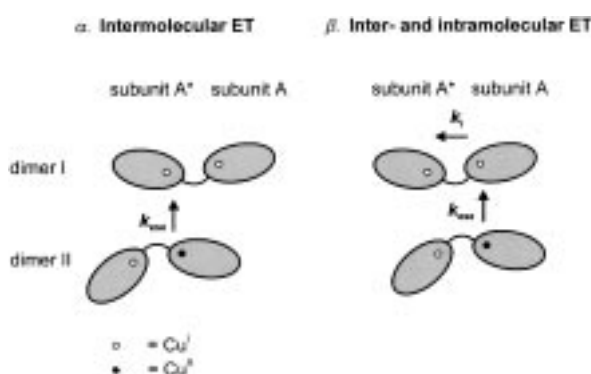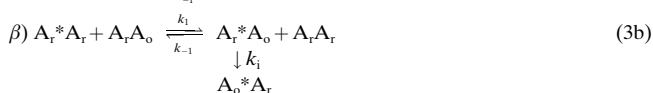
$$\alpha)\ A_r*A_r + A_rA_o \underset{k_{-1}}{\overset{k_1}{\rightleftharpoons}} A_o*A_r + A_rA_r \tag{3a}$$

$$\beta)\ A_r*A_r + A_rA_o \underset{k_{-1}}{\overset{k_1}{\rightleftharpoons}} A_r*A_o + A_rA_r \tag{3b}$$
$$\downarrow k_i$$
$$A_o*A_r$$

Figure 2. Schematic representation of possible hole transfer routes in N42C azurin dimers. α) Subunit A* of dimer I becomes oxidized by intermolecular hole transfer from dimer II to dimer I with rate constant k_{ese}. β) Subunit A* of dimer I is oxidized by two consecutive steps, a) intermolecular hole transfer from dimer II to subunit A of dimer I at rate constant k_{ese}, b) intramolecular hole transfer within dimer I from subunit A to subunit A* at rate k_i. The arrows denote the flow of the unpaired spin, the transfer of the electron occurs in the opposite direction.

The line-broadening, from which the rate constants are deduced, is determined by the probability of the Cu^I site to become oxidized, which causes the nearby proton spin to loose its phase coherence before it is lost due to relaxation mechanisms. Once the A_r* moiety has become oxidized, back reactions are irrelevant for the broadening process. The overall rate, k_{obs}, by which A_r*A_r is converted into A_o*A_r, is now the sum of the contributions from the processes (α) and (β), which are given by Equation (4):

$$k_\alpha = k_{ese}[A_oA_r] \tag{4a}$$

$$k_\beta = k_{ese}[A_oA_r] \cdot \left[\frac{k_i}{k_{ese}[A_rA_r] + k_i} \right] \tag{4b}$$

The overall rate is given by Equation (5):

$$k_{obs} = k_\alpha + k_\beta = k_{ese}[A_oA_r] \cdot \left[1 + \frac{k_i}{k_{ese}[A_rA_r] + k_i} \right] \tag{5}$$

The symbols k_{ese} and k_i represent the inter- and intramolecular electron transfer rate constant, respectively.

To discriminate between the intra- and intermolecular electron transfer, the e.s.e. rate constant was determined not only for (Cu–Cu) azurin dimers, but also for azurin dimers that contain one Zn and one Cu ion. In the latter case, intramolecular electron transfer is absent, because Zn^{II} is redox-inactive. Therefore, the intermolecular rate constant, k_{ese}, for this (Zn^{II}–Cu)-N42C dimer can be calculated using Equation (4a), and is identical to the intermolecular electron transfer rate constant for (Cu–Cu)-azurin dimers. A possible charge effect of the metals in the azurin dimer on the rate constant has been examined by determining the electron transfer properties of (Ag^I–Cu)-N42C dimers as well. Finally, an upper limit for the intramolecular rate constant, k_i, can be derived by measuring k_{obs} at different total protein concentrations while the percentage of oxidized protein is kept fixed.

Results

(Cu–Cu)-N42C Azurin dimer—Isolation, characterization, and dimer formation: The mutated azurin, N42C, was grown and isolated as described in the Experimental Section. An average 7 mg of apo-N42C azurin per liter of culture was obtained. Compared with the yields that are normally obtained for wild-type azurin (15–30 mg L^{-1}), this yield is low. This is probably due to the reactivity of the cysteine introduced at position 42 and the formation of aggregates with other components in the cell lysate. Increasing the concentration of dithiotreitol (DTT) during the isolation did not improve the yields, however.

Holo-N42C azurin was obtained by adding a slight excess of $Cu(NO_3)_2$ after the removal of DTT, which resulted in the appearance of the characteristic blue color of azurin. The copper was partially reduced, because of the formation of disulfide bonds, which resulted in a 75% conversion of the mutant into dimer. The addition of a small excess of potassium ferricyanide resulted in the conversion to 100% dimer and re-oxidation of the copper. The presence of the (Cu–Cu)-N42C dimer was confirmed by gel filtration and electrospray mass spectrometry (results not shown). The experimentally determined mass of the holo-N42C azurin dimer was 27 983 (± 8), while the calculated mass is 27 990. In addition, SDS-PAGE, native and iso-electric focussing (IEF) electrophoresis confirmed the appearance of the (Cu–Cu)-N42C azurin dimer (see Figure 3).
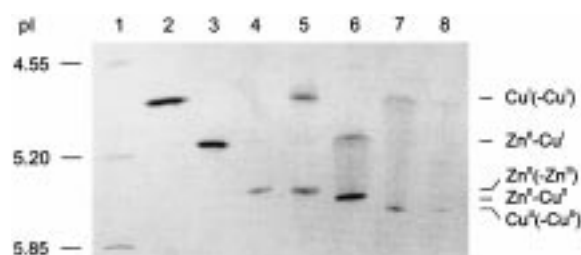

Figure 3. IEF gel electrophoresis of (N42C) azurin samples. Lane 1: pI marker proteins; lane 2: (Cu^I–Cu^I)-N42C azurin dimer; lane 3: (Zn^{II}–Cu^I)-N42C azurin dimer that is obtained by reduction of the (Zn^{II}–Cu^{II})-N42C azurin dimer with ascorbate; lane 4: (Zn^{II}–Zn^{II})-N42C azurin dimer; lane 5: Zn^{II}- and Cu^I-N42C azurin monomers obtained by reduction of the (Zn^{II}–Cu^{II})-N42C azurin dimer with DTT; lane 6: (Zn^{II}–Cu^{II})-N42C azurin dimer; lane 7: (Cu^{II}–Cu^{II})-N42C azurin dimer; lane 8: Cu^{II} wild-type azurin. In lanes 6, 7 and 8, partial back-reduction has occurred in the gel.

The number of free thiol groups was determined with the use of Ellman's reagent (5,5′-dithiobis-(2-nitrobenzoic acid), DTNB).[39] The results are listed in Table 1. Under native conditions, no free cysteines were detected in the N42C holo-dimer, whereas, in the apo-monomer, one cysteine was

Table 1. Cysteine reactivity of wild-type and N42C azurin.

| | Reactive cysteine/azurin [mol/mol][a] | |
	Native[b]	Denatured[c]
wild-type		
apo	0	1.0
Cu	0	0.9
N42C		
apo-monomer	1.0	1.6
Cu-monomer	0.6	1.2
Cu-dimer	0	1.5

[a] Protein concentrations were calculated from A_{280} with the use of $\varepsilon_{280} = 9.8\,\text{mm}^{-1}\text{cm}^{-1}$ and varied from 10–50 μM. A 100-fold excess of DTNB was used. Errors in reactive cysteine/azurin are ±0.1. [b] Reactions were performed in 20 mM HEPES, pH 7. [c] Reactions were performed in 6 M guanidinium chloride, 10 mM EDTA.

reactive to DTNB. The holo-monomer, which was obtained by reaction of the dimer with DTT followed by removal of excess DTT, showed only 0.6 (±0.1) free thiol groups. Presumably, monomer was partially re-oxidized to dimer during sample preparation. Wild-type azurin, used as a control, did not exhibit any free thiol groups in either its apo- or its holo-form under native conditions. When the proteins were denatured in 6 M guanidinium chloride, in the presence of EDTA (10 mM) to prevent copper-induced dimerization, 1.5 (±0.1) free cysteines (per dimer) were determined in the N42C holo-dimer. For the apo- and holo-monomer, 1.6 (±0.1) and 1.2 (±0.1) cysteines, respectively, were titratable in the denatured form. In wild-type azurin, one thiol group (Cys112) was reactive towards DTNB under denaturing conditions. From these observations, it can be concluded that, in the monomeric N42C azurin, surface-exposed Cys42 is reactive towards DTNB under native conditions, whereas, under denaturing conditions, Cys112 also becomes exposed in both the monomeric and dimeric form and reacts with DTNB.

The UV/Vis absorption spectrum as well as the EPR spectrum of oxidized N42C azurin dimer are identical to those of wild-type azurin ($\lambda_{\text{max}} = 628$ nm, $\varepsilon_{628} = 5.7\,\text{mm}^{-1}\text{cm}^{-1}$; $g_{\parallel} = 2.26$, $g_{\perp} = 2.05$ and $A_{\parallel} = 57 \times 10^{-4}\,\text{cm}^{-1}$), which indicates that no structural changes around the copper site have occurred. The one dimensional ^{1}H NMR spectrum of N42C dimer is very similar to that of wild-type azurin, except for some line broadening (3–4 Hz) as a result of the larger rotational correlation time of the dimer (see Figure 4).

(Zn–Cu)-N42C Azurin dimer—Isolation, characterization, and dimer formation: Zn-N42C azurin was isolated as a by-product of the isolation of apo-N42C azurin. Typically, 4.5 mg of Zn-azurin was obtained per liter of cell culture. (Zn–Cu)-dimers of N42C azurin were obtained by the oxidation of a solution that contains a 1:1 mixture of Cu- and Zn-N42C
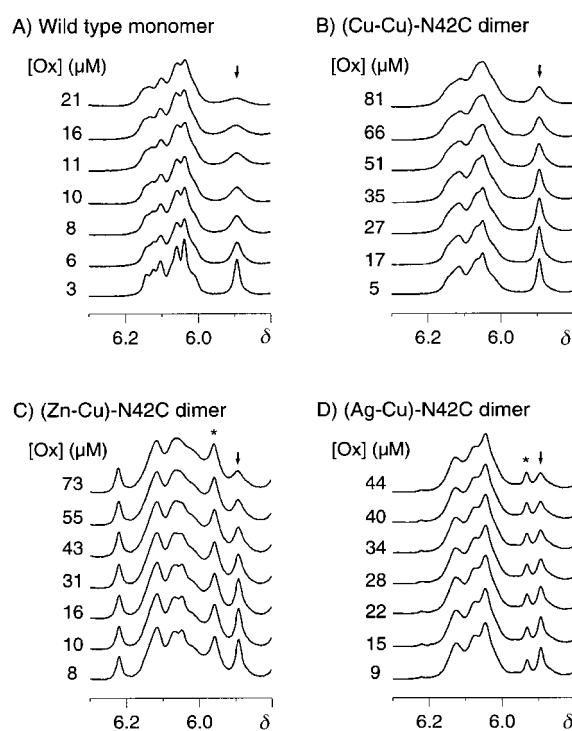

Figure 4. Electron self-exchange (e.s.e.) measurements. Region of the 600 MHz ^{1}H NMR spectra at $T = 313$ K and pH* 8.5 of A) wild-type azurin, B) (Cu–Cu)-N42C azurin dimer, C) (Zn–Cu)-N42C azurin dimer and D) (Ag–Cu)-N42C azurin dimer, that shows the His46 C$^{\delta 2}$H signal at $\delta = 5.89$ (arrow) used for determining the line-broadening as a function of the concentration of oxidized azurin (in μM). The total protein concentration is 1 mM. (*) denotes the His46 resonance for Zn- and Ag-sites in the (Zn–Cu)- and (Ag–Cu)-dimers, respectively.

monomers as described in the Experimental Section. The formation of (Zn–Cu)-dimers was followed by IEF electrophoresis (Table 2 and Figure 3). The pI of the (Zn$^{\text{II}}$–Cu$^{\text{I}}$)-azurin dimer was determined to be 5.16 (Figure 3, lane 3), which is the average of the pI of (Cu$^{\text{I}}$–Cu$^{\text{I}}$)-azurin and (Zn$^{\text{II}}$–Zn$^{\text{II}}$)-azurin, 4.87 and 5.49, respectively (Table 2 and Figure 3, lanes 2 and 4). The pI values of the apo-, (Cu–Cu)- and (Zn–Zn)-N42C dimers are the same as the pI values of the apo-, Cu- and Zn-wild-type monomers, respectively. This is shown for the Cu$^{\text{II}}$ case in Figure 3, lanes 7 and 8. Oxidized (Zn$^{\text{II}}$–Cu$^{\text{II}}$)-azurin dimer (lane 6) has a pI of 5.56, which is between the pI of (Zn$^{\text{II}}$–Zn$^{\text{II}}$)-azurin and (Cu$^{\text{II}}$–Cu$^{\text{II}}$)-azurin (5.49 and 5.65, respectively). Mild reduction of the (Zn$^{\text{II}}$–Cu$^{\text{II}}$) dimer

Table 2. pI values of different forms of wild-type and N42C azurin.[a]

| | pI[b] | |
	Wild-type	N42C
apo	5.90 (0.02)	5.90 (0.02)
Cu$^{\text{II}}$(–Cu$^{\text{II}}$)	5.65 (0.03)	5.65 (0.03)
Cu$^{\text{I}}$(–Cu$^{\text{I}}$)	4.87 (0.03)	4.87 (0.03)
Zn$^{\text{II}}$(–Zn$^{\text{II}}$)	5.49 (0.02)	5.49 (0.02)
Zn$^{\text{II}}$–Cu$^{\text{I}}$	–	5.16 (0.03)
Zn$^{\text{II}}$–Cu$^{\text{II}}$	–	5.56 (0.04)
Ag$^{\text{I}}$–Cu$^{\text{II}}$	–	5.16 (0.03)
Ag$^{\text{I}}$–Cu$^{\text{I}}$	–	4.87 (0.03)

[a] IEF was performed with polyacrylamide gels (PhastGel) with a pH gradient of 4–6.5. [b] pI values were determined from a comparison with marker proteins from Pharmacia.

with an equimolar amount of ascorbic acid converts the dimer into the reduced (Zn^{II}–Cu^I) form (Figure 3, lane 3). Reduction with DTT results in the breakage of the disulfide bond, which is shown by the formation of separate Zn^{II} and Cu^I monomers (Figure 3, lane 5).

The (Zn^{II}–Cu^I)-dimer was separated from the other components with the use of anionic exchange chromatography as described in the Experimental Section. Five peaks were obtained, most of which were well resolved. The first two peaks, one as a shoulder on a third peak, were monomer fractions that were not further used. The next three major peaks, which contain (Zn^{II}–Zn^{II})-dimer, (Zn^{II}–Cu^I)-dimer and (Cu^I–Cu^I)-dimer, respectively, were well resolved from each other. Fractions were pooled, concentrated and analyzed by IEF. The (Zn–Cu)-dimer was > 95 % pure as judged by IEF, a spectral A_{628}/A_{280} ratio of 0.28 and gel filtration.

The one-dimensional ^1H NMR spectrum of (Zn–Cu)-N42C dimer shows the doubling of several resonances as compared with the spectrum of (Cu–Cu)-N42C dimer, among which the $C^{\delta 2}H$ resonance of the Cu ligand His46 (see Figure 4C). This is the consequence of the two histidines 46 in the (Zn–Cu)-dimer no longer being equivalent, that is one His46 is close to Cu^I, while the other is close to Zn^{II}, which results in different chemical shifts for the His46 resonances.[40]

(Ag–Cu)-N42C Azurin dimer—Isolation, characterization, and dimer formation: The (Ag–Cu)-N42C dimer was obtained as described in the Experimental Section. The protein was > 95 % pure as judged by IEF (pI 5.16 for (Ag^I–Cu^{II})-N42C azurin) and the spectral A_{628}/A_{280} ratio of 0.28. The one-dimensional ^1H NMR spectrum also shows doubling of several resonances compared with that of (Cu–Cu)-N42C dimer as can be seen in Figure 4D. However, the effect is less pronounced than in the (Zn–Cu)-dimer.

Electron self-exchange measurements: The e.s.e. rate constants of wild-type, (Cu–Cu)-, (Zn–Cu)- and (Ag–Cu)-N42C azurin were determined from the line-broadening (ΔT_2^{-1}) of the $C^{\delta 2}H$ resonance of the Cu-ligand His46 ($\delta =$ 5.89) in the NMR spectra of the reduced protein as a function of the Cu^{II} azurin concentration in the sample, as illustrated in Figures 4 and 5. The position of the His46 $C^{\delta 2}H$ resonance depends on pH, that is $\delta = 5.55$ at low pH and $\delta = 5.89$ at high pH. This variation in peak position is due to a local conformational change of the protein that is connected with the deprotonation of His35,[31, 36] and is not relevant for our study. It has been previously shown that pH variations do not significantly affect the e.s.e. rate constant of *P. aeruginosa* azurin.[36] Therefore, we chose to measure at pH 8.5; at this pH, the His46 $C^{\delta 2}H$ resonance is well resolved from other resonances. Upon addition of small amounts of oxidized protein, the resonance of His46 which coordinates to the copper is affected by the paramagnetism of Cu^{II}, which results in conspicuous line-broadening, especially for wild-type azurin (see Figure 4). When plotting the linewidth against concentration of oxidized azurin, k_{ese} can be obtained from the slope (see Equation 2 and Figure 5). The data are summarized in Table 3. The e.s.e. rate constants for the dimers [(Cu–Cu), (Zn–Cu) and (Ag–Cu)] are seven times
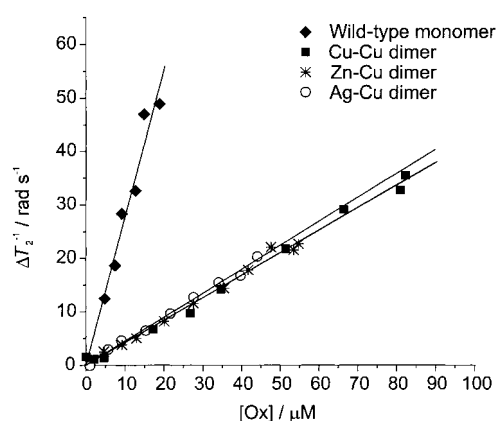

Figure 5. Line-broadening, ΔT_2^{-1} (in rad s^{-1}), of the His46 $C^{\delta 2}H$ resonance as a function of the concentration of oxidized azurin (μM). Measurements were performed at pH* 8.5, $T = 313$ K and total protein concentrations of 1 mM. ◆ = wild-type azurin, ■ = (Cu–Cu)-N42C azurin dimer, ✳ = (Zn–Cu)-N42C azurin dimer, ○ = (Ag–Cu)-N42C dimer.

Table 3. Electron self-exchange rate constants of wild-type and N42C azurins.

	k_{ese} (10^5 M^{-1}s^{-1})[a]			
[Azu] (mM)	Wild-type	(Cu–Cu)-N42C	(Zn–Cu)-N42C	(Ag–Cu)-N42C
1.0	28 (5)	4.2 (0.7)	4.2 (1.0)	4.5 (1.0)
0.7	29 (6)	4.1 (0.5)	4.2 (0.5)	n.d.[b]
0.5	25 (7)	3.9 (0.5)	4.2 (0.7)	n.d.
0.3	23 (10)	3.6 (0.6)	4.5 (1.1)	n.d.

[a] Conditions: 25 mM potassium phosphate in D$_2$O, pH* 8.5, $T = 313$ K. [b] n.d. = not determined.

smaller than the k_{ese} of wild-type azurin, that is 4.2(± 0.7) $\times$ 10^5 M^{-1}s^{-1}, 4.2(± 1.0) $\times$ 10^5 M^{-1}s^{-1}, and 4.5(± 1.0) $\times$ 10^5 M^{-1}s^{-1}, respectively, versus 28(± 5) $\times$ 10^5 M^{-1}s^{-1} for wild-type azurin. The similarity of the k_{ese} rate constants of (Cu–Cu)-, (Zn–Cu)- and (Ag–Cu)-N42C dimers shows that the contribution from process β to the overall e.s.e. rate of the (Cu–Cu)-dimers is small. In addition, the similarity between the rates demonstrates that the effect of the metal's charge is negligible.

In order to determine an upper limit for k_i in (Cu–Cu)-dimers, the total protein concentration was varied. While the ratio of oxidized to total protein was kept fixed at 0.08, line broadening ($= k_{obs}$) was measured at different total protein concentrations. Figure 6 shows how the calculated value of $k_{obs}/(k_{ese}[A_rA_o])$ [see Eq. (6)] varies as a function of [A_rA_r] for values of k_i that range from 0 to 10^3 s^{-1}.

$$k' \equiv \frac{k_{obs}}{k_{ese}[A_rA_o]} = 1 + \frac{k_i}{k_{ese}[A_rA_r] + k_i} \qquad (6)$$

The experimental data in Figure 6 show that $k_i < 10$ s^{-1}.

Modelling studies: In order to obtain more insight into the relative orientation of the two monomers and the Cu–Cu distance, modelling studies were performed with the use of X-PLOR 3.1.[41] As mentioned in the Introduction, the azurin molecules are packed two by two with their hydrophobic patches facing each other in the crystal. The packing is such that the residues at position 42 in the hydrophobic patch can almost make van der Waals contact. Modelling was started by
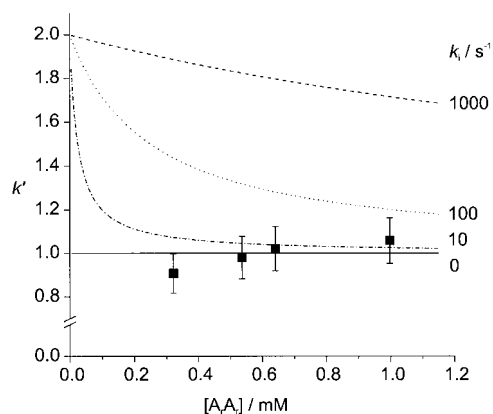
Figure 6. Determination of an upper limit for the intramolecular electron transfer rate in the (Cu–Cu)-N42C azurin dimer. k' ($\equiv k_{obs}/(k_{ese}[A_rA_o])$) is plotted versus the concentration of reduced azurin, $[A_rA_r]$ (in mM), for $k_i = 1000$ (– – –), 100 (•••), 10 (•–•–) and 0 (——) s^{-1} using Equation (6). ■ = experimental values of k' for the (Cu–Cu)-N42C dimer at pH* 8.5, $T = 313$ K; the degree of oxidation equals 8%.
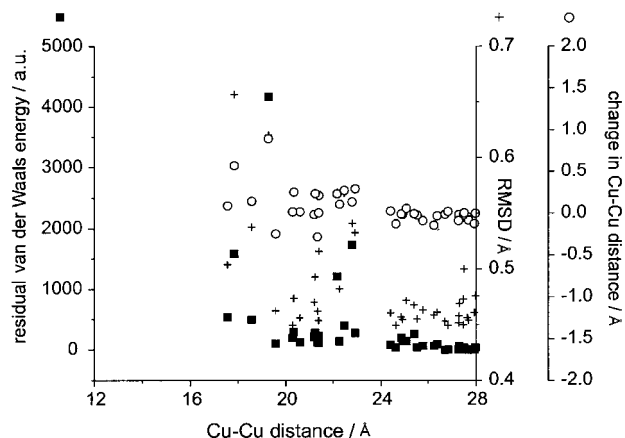

Figure 7. Correlation between the Cu–Cu distance of N42C azurin dimers and the residual van der Waals energy (a. u.) of 40 rotamer structures that were minimized for the contact between monomers generated by X-PLOR. Left scale: the residual van der Waals energy (a. u.) (■); right scale: change in Cu–Cu distance in Å after minimization (○); RMSD value in Å between the heavy atoms before and after minimization (+).

taking the coordinates of two azurin molecules, which we shall denote as A and B, from the crystal structure and building a Cys–Cys link at positions 42 in the amino acid chain. As there are then five covalent bonds that connect the amino acid chain of azurin molecule A with the chain of molecule B, there are five dihedral angles, which specify the orientation of molecule A with respect to B.

We wished to know which combinations of dihedral angles would have no steric hindrance between A and B. To sample the "dihedral angle space" spanned by these five dihedrals, the five bonds that connect the two cysteines from C_α (Cys42, subunit A) to C_α (Cys42, subunit B) were systematically rotated over angles of 60, 180 and 300 degrees, while the rest of the protein was kept unchanged. This resulted in 108 non-symmetry related rotamer structures, for which the van der Waals energy between the two "monomers" was calculated. From these structures, those with severe backbone collisions between the monomers were eliminated, as were those that demonstrated van der Waals overlap between the atoms of the Cys42 residues. The remaining 40 structures were energy-minimized to relieve minor steric collisions. In the calculations, the coordinates of the Cys42 residues were fixed to maintain the relative orientation of the monomers. Figure 7 illustrates the correlation between the residual van der Waals energy and the Cu–Cu distance of these 40 minimized rotamers. In Figure 8, the structures are grouped in a histogram that counts the number of structures that correspond with a particular Cu–Cu distance ±0.5 Å.

From these figures, it can be seen that all of the generated structures have a Cu–Cu distance >17 Å, and most of them >20 Å. The Cu–Cu distance in the minimized structures is not significantly changed relative to the rotamers before minimization, as can be seen in Figure 7 as well. Rotamers with a relatively short Cu–Cu distance are more affected by minimization than those with a larger Cu–Cu distance. This is also reflected in the root-mean-square difference (RMSD) between the heavy atoms before and after minimization: Rotamers with a relative short Cu–Cu distance have a relative high RMSD value. These effects illustrate the
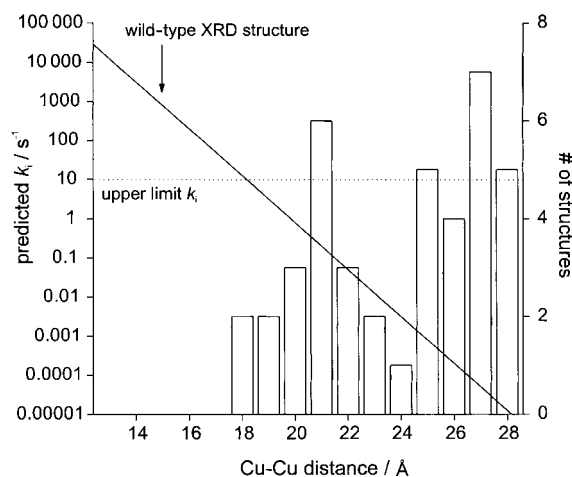

Figure 8. Histogram of 40 energy minimized structures of the N42C dimer in order of their Cu–Cu distance. The solid line represents the correlation given by Equation (7) between the predicted intramolecular electron transfer rate k_i (s^{-1}) and the Cu–Cu distance. The experimental upper limit for the intramolecular electron exchange of 10 s^{-1} is indicated by a dotted line. This value corresponds with a Cu–Cu distance of 18 Å. All 40 minimised structures comply with this distance. The arrow denotes the Cu–Cu distance in the crystal structure of wild-type azurin.

relatively large steric overlap in the structures with small Cu–Cu distances before minimization. To minimize this overlap, the monomers move away from each other during the minimization process.

Discussion

The measured intermolecular e.s.e. rate constants of wild-type azurin and N42C azurin dimers are summarized in Table 3. The previously determined rate constant of $2.1(\pm 0.1) \times 10^6$ M^{-1}s^{-1} measured for wild-type azurin at comparable conditions (20 mM potassium phosphate, pH 9, $T = 309$ K)[36] agrees with the value of wild-type azurin reported herein (25 mM potassium phosphate, pH 8.5, $T = 313$ K). The difference in the intermolecular e.s.e. rate constant between wild-

type azurin $(28(\pm 5) \times 10^5\,\mathrm{M}^{-1}\mathrm{s}^{-1})$ and the N42C dimer $(4.2(\pm 0.7) \times 10^5\,\mathrm{M}^{-1}\mathrm{s}^{-1})$ is ascribed to a less accessible hydrophobic patch in the dimer, which is due to steric hindrance as a result of the introduction of the covalent link between the two patches. Still, this relatively high rate constant of $4.2 \times 10^5\,\mathrm{M}^{-1}\mathrm{s}^{-1}$ indicates that the hydrophobic patch is accessible for inter-protein electron transfer. Thus, the monomers are not tightly packed with their hydrophobic patches facing each other.

The similarity of the intermolecular e.s.e. rate constants of the (Cu–Cu)-, (Zn–Cu)- and (Ag–Cu)-N42C dimers is accompanied by a very slow intramolecular electron transfer rate of $k_i < 10\,\mathrm{s}^{-1}$ as determined in the dilution experiment. It is interesting to compare this upper limit with that predicted for k_i from a semi-empirical equation [see Eq. (7)] for non-adiabatic electron transfer in proteins:[42]

$$\log k_{et} = 15 - 0.6R - 3.1(\Delta G + \lambda)^2/\lambda \qquad (7)$$

The distance between the redox centers, R, is expressed in Å, the free energy, ΔG, and the reorganization energy, λ, are in eV.

Equation (7) is in agreement with a large body of experimental data albeit that the spread of the experimental points around the correlation line presented by Equation (7) equals two orders of magnitude. Strictly speaking, moreover, Equation (7) applies to intra-protein electron transfer, while we are considering electron transfer events in which the solvent may play a role. In the case of azurin, it has been pointed out that the pathway of the e.s.e. reaction may involve two water molecules that are connected by hydrogen bridges and link the N^ε atoms of the His117 side chains in the hydrophobic patches of the molecules in the association complex. The His117 imidazole moiety directly coordinates to the Cu. The two water molecules have been identified in the crystal structure.[26, 27] For complexes of this type, it is thought that Equation (7) can still be used to analyze electron transfer data.

Using $\Delta G = 0$, a Cu–Cu distance of 15 Å, as found in the crystal structure of wild-type azurin, and an estimated value for λ of 1 eV $(99.4 \pm 5\,\mathrm{kJ\,mol}^{-1})$,[43] we calculate a k_{et} of approximately $800\,\mathrm{s}^{-1}$. An increase of the Cu–Cu distance by a few angstroms dramatically decreases the electron transfer rate. For example, a 5 Å increase in R leads to a 1000-fold decrease in the electron transfer rate. This suggests that the two copper centers in a N42C azurin dimer are, on average, further apart than in the crystal structure of wild-type azurin (>18 Å versus 15 Å), and that the introduction of a covalent disulfide bond between the two subunits hinders the formation of a complex with fast intramolecular electron transfer, despite the apparently favourable position of N42C for dimer formation in the crystal structure (Figure 1). Furthermore, the conformation of the dimer may no longer allow for an electronic coupling pathway that involves a few bridging water molecules, thus weakening the electronic coupling and lowering the e.s.e. rate.

The alternative explanation that the two azurin molecules keep the same orientation as in the crystal structure, but that the reorganization energy has increased, is less likely. To be

compatible with a decrease by a factor of 10^3 in rate, the reorganization energy would have to increase from 1.0 eV to 2.0 eV. This is outside the range of λ values encountered for electron transfer reactions of blue copper proteins. Experimental work has established, for example, that the reorganization energy of *Pseudomonas aeruginosa* azurin is ~ 0.7 eV.[44]

The modelling studies reported in Figure 7 support these conclusions, that is an increase of the distance between the two coppers is found in comparison with the crystal structure of wild-type azurin. In Figure 8, the correlation given by Equation (7) is presented by a solid line. The arrow indicates the point where $R = 15$ Å, the Cu–Cu distance found in the crystal structure of wild-type azurin. It is clear from this figure that an upper limit of $k_i < 10\,\mathrm{s}^{-1}$ (dotted line) is compatible with structures in which the Cu–Cu distance is larger than 18 Å. All accessible rotamers fall in this category.

Further support for this analysis comes from X-ray diffraction studies. Crystals of the N42C dimer could be obtained and an X-ray data set that extends to 2.6 Å resolution was collected with synchrotron radiation at DESY in Hamburg. The molecular replacement method using program AMoRe[45] and one azurin molecule as search model provided one prominent solution. The solution shows the N42C dimers arranged in the crystal as two dimers, not in a head-to-head fashion as one would expect, but in an oblique manner. The Cu–Cu distance in the dimer is approximately 25.9 Å (X-ray structure analysis, O. Einsle and A. Messerschmidt, unpublished results), in accordance with our data.

Conclusion

The work presented herein deals with the electron transfer kinetics of azurin dimers that were constructed by introducing a well-defined site for covalent cross-linking into the azurin structure. A seven-fold decrease in the bimolecular e.s.e. rate constant of (Cu–Cu)-, (Zn–Cu)- and (Ag–Cu)-N42C azurin dimers was found compared with the rate constant of wild-type azurin, which is ascribed to a less accessible hydrophobic patch in the dimers. An upper limit for the intramolecular electron transfer in (Cu–Cu)-dimers was determined to be $10\,\mathrm{s}^{-1}$, which means that the predominant conformation(s) of the two azurin moieties in the dimer must be different from the mutual orientation that two azurin molecules display in the crystal structure of wild-type azurin. Apparently, the introduction of the Cys42–Cys42 disulfide bond causes the two azurin molecules to adopt a conformation around the Cys–Cys link that weakens the electronic coupling between the redox centers as compared with the association complex of two azurin monomers in solution. Modelling studies as well as X-ray structure analysis are in agreement with an increase of the distance between the two coppers when compared with the crystal structure of wild-type azurin. The results show that electron transfer in protein–protein complexes depends crucially on subtle structural details and, for efficient electron transfer, it is vitally important that the molecules form a complex with the proper conformation. The present study shows that cross-linking with short linkers (e.g. an engineered

disulfide bond) may result in the fixation of protein complexes whose conformations have no physiological relevance.

Experimental Section

Bacterial strains and plasmids: *Escherichia coli* strain JM109 was used for cloning and expression of the *Pseudomonas aeruginosa azu* gene. The plasmid pGK22 was a kind gift from Dr. B. G. Karlsson (Chalmers University of Technology, Gothenburg, Sweden), and was used for the mutagenesis and over-expression of the *azu* gene under the control of the *lac* promoter. The plasmid was slightly modified resulting in plasmid pIA01 in order to generate a unique SalI site that could be used for cloning.

Site-directed mutagenesis: The Asn42 → Cys mutation was introduced into the *azu* gene by the three-step PCR mutagenesis protocol as described by Picard et al.[46] The oligonucleotide used for construction of the Asn42 → Cys mutation was 5′-CCTGCCGAAG*TG*CGTCATGGG*T*CA-CAACTGGG-3′. (Bold *TG* represents the double mismatch necessary for the mutation and single bold *T* indicates a silent mutation, introduced for screening purposes, i.e., HaeIII deletion). The downstream and upstream primers were chosen to be close to the unique KpnI and SalI site of pIA01, respectively. These restriction sites were used to insert the KpnI/SalI digested PCR fragment into the pIA01 plasmid, and thus to replace part of the wild-type *azu* gene, which generates plasmid pIA02. Screening was performed by restriction analysis that used HaeIII as a restriction enzyme. Finally, sequence analysis of the complete *azu* gene confirmed the mutation.

Protein isolation, purification, **and characterization**: Wild-type and N42C azurin were isolated from *E. coli* JM109 cells, and transformed with plasmids pGK22 and pIA02, respectively. Cells were grown overnight and diluted 1:100 in 30 L of Luria-Bertani (LB) medium supplemented with 100 µg mL^{-1} ampicillin and 27 µg mL^{-1} isopropyl-β-thiogalactopyranoside (IPTG) in a 40 L fermentor (MPP40; New Brunswick Scientific, Edison, NJ). The cells were harvested directly at the end of the exponential growth phase by filtration with the use of a Pellicon cassette filter (Millipore). Wild-type azurin was isolated as previously described.[47] A few modifications were introduced in the purification procedure for N42C azurin. It was isolated in the apo-form, and no Cu^{II} or K$_3$[Fe(CN)$_6$] was added after the osmotic shock. Instead, dithiotreitol (DTT, 3–5 mM) was added. DTT was also added in all further isolation and purification steps to prevent aggregation with other proteins and small molecules that contained sulfide.

(Cu–Cu)-N42C Azurin dimers were rapidly formed when the apo-form was incubated with Cu^{II}, which acts as a catalyst for disulfide formation. Typically, 1.1 molar equivalents of a Cu(NO$_3$)$_2$ solution and an excess (5 molar equivalents) of K$_3$[Fe(CN)$_6$] were added to an apo-N42C azurin solution in 20 mM HEPES, pH 7, to obtain 100% of the (Cu^{II}–Cu^{II})-dimer. Free thiol groups were assayed with Ellman's reagent (5,5′-dithiobis-(2-nitrobenzoic acid), DTNB, purchased from Aldrich) by monitoring the absorbance at 412 nm of thionitrobenzoate. Moles of free -SH were calculated from the molar extinction coefficient of thionitrobenzoate ($\varepsilon_{412} = 13700$ M^{-1} cm^{-1} in 6 M guanidine hydrochloride and 14150 M^{-1} cm^{-1} in its absence).[39] Absorption spectroscopy was performed either on a Shimadzu UV 2101PC or a Perkin–Elmer Lambda 18 spectrophotometer.

(Zn–Cu)-N42C Azurin dimers were prepared by mixing monomeric Cu-N42C and monomeric Zn-N42C azurin in a 1:1 ratio in the presence of 10 mM DTT. Zn-N42C azurin was obtained as a by-product of the apo-N42C azurin preparation.[47, 48] To allow the formation of dimers by oxidation in air, DTT was slowly removed by dialysis. The different dimers (Cu^I–Cu^I, Zn^{II}–Cu^I and Zn^{II}–Zn^{II}) and small amounts of monomer that were still present were separated with the use of a Q-sepharose column that was connected to an FPLC system (Pharmacia). The difference in the charge of the components made it possible to separate the (Zn^{II}–Cu^I)-N42C dimer from the other components. A small amount of ascorbic acid, low enough to prevent the conversion of dimer into monomer, was added to keep the copper in its reduced state before loading the sample onto the Q-sepharose column. Subsequently, the column was eluted with a salt gradient from 0–45 mM NaCl in 20 mM Tris, pH 8, at a rate of 6 mL min^{-1}.

(Ag–Cu)-N42C Dimers were obtained in a similar way as (Zn–Cu)-N42C dimers, except for the anion exchange chromatography, which in this case

was performed under oxidizing conditions to enable the separation of the different dimers (Cu^{II}–Cu^{II}, Ag^I–Cu^{II} and Ag^I–Ag^I). Ag-N42C azurin was produced by incubating apo-N42C azurin with a small excess of Ag(NO)$_3$.

Gel filtration on a Superdex 75 column (length 60 cm, ∅1.6 cm) connected to an FPLC system (Pharmacia) was used as a purification step as well as for qualitative analysis. A buffer solution that contained 20 mM HEPES, 0.15 M NaCl at pH 7 was used. The purity of the proteins was determined by their optical A_{628}/A_{280} ratios (≥ 0.55 for (Cu–Cu)-N42C dimers and 0.27 $\geq$ ratio ≤ 0.30 for (Zn–Cu)- and (Ag–Cu)-N42C dimers) as well as from IEF (Pharmacia PhastSystem), sodium dodecyl sulfate-polyacrylamide gel electrophoresis (SDS-PAGE) and native gel electrophoresis.

Gel electrophoresis: Denaturing SDS-PAGE was performed with 15% polyacrylamide gels (Laemmli system) that used a mini-vertical electrophoresis system of BIORAD. Samples were dissolved in standard buffer solutions and heated for five minutes prior to loading the gel. Native gel electrophoresis was performed as SDS-PAGE, but in the absence of SDS and β-mercaptoethanol and without heating the samples. IEF was performed with polyacrylamide gels (PhastGel) in which a pH gradient of 4–6.5 was established with the use of a Pharmacia PhastSystem (Amersham Pharmacia Biotech, Uppsala, Sweden). pI values were determined from a comparison with marker proteins from Pharmacia.

Protein samples for NMR: For the e.s.e. rate constant determinations, the protein was exchanged into 99.9% deuterated 25 mM potassium phosphate buffer, pH* 8.5 with the use of Amicon ultrafiltration equipment. The pH was not corrected for the deuterium isotope effect, and is denoted as pH*. Samples were typically 1 mM in total protein concentration. Reduced protein samples were obtained by incubation with one equivalent of ascorbic acid, which was subsequently removed by repeated concentration and dilution with the use of an Amicon ultrafiltration cell. Argon was passed through all buffers and protein solutions prior to use to prevent reoxidation. Partially oxidized samples were obtained by adding small amounts of Cu^{II} protein to the reduced protein (both at the same stock concentrations). The concentration of oxidized protein in the samples was measured with a special sample holder, which was designed such that the absorbance of the protein solution could be measured at 628 nm in the NMR tube on a Perkin–Elmer Lambda 18 spectrophotometer that used optical fibers (Hellma, Müllheim/Baden, Germany). The concentration of oxidized azurin, expressed as the concentration of oxidized copper sites, [Cu^{II}], was measured before and after recording the NMR spectrum that used $\varepsilon_{628} = 5.7$ mM^{-1} cm^{-1}. The average of the two values was used in the calculations. Values of T_2^{-1} for the C$^{\delta 2}$H resonance of His46 (at $\delta = 5.89$) were obtained by multiplying the peak width at half height by π ($T_2^{-1} = \pi\nu_{1/2}$) and were plotted against the concentration of oxidized protein in the sample. From the slope of this plot, the self-exchange rate constant was determined. The dependence of the e.s.e. reaction on the concentration of reduced protein was investigated with the use of an approximately 8% oxidized protein sample in the case of the dimers and a 2% oxidized sample for the wild-type monomeric azurin. Protein solutions were diluted in steps that started at 1 mM up to 0.7 mM, 0.5 mM and 0.3 mM, subsequently. The broadening of the C$^{\delta 2}$H resonance of His46 was measured relative to its width in a fully reduced sample.

NMR spectroscopy: ^{1}H NMR spectra were acquired on a Bruker Avance DMX 600 MHz spectrometer at 313 K. The spectral width was 12.98 ppm. Free induction decays were accumulated in 4 K memory and Fourier-transformed with the use of a QSINE window function. The chemical shifts were calibrated with the use of sodium 3-(trimethylsilyl)propionate (TSP, 200 µM) as an internal reference.

Modelling: In the crystal structure of wild-type azurin, two azurin molecules face each other with opposing hydrophobic patches. Using INSIGHT II, the asparagines 42 in this structure were replaced by cysteines, which enabled the introduction of a disulfide bond. The dimer structure was used as the starting point for the modelling studies. With X-PLOR 3.1[41] the five bonds that connect the two cysteines from C$_\alpha$ (Cys42, subunit A) to C$_\alpha$ (Cys42, subunit B) were rotated systematically over angles of 60, 180 and 300 degrees, while keeping the rest of the protein unchanged. Energy minimization was performed on rotamer structures that showed no or small steric overlap between the two separate monomers or within the Cys42 residues, as determined by visual inspection. The coordinates of the Cys42 residues were fixed to maintain the relative orientation of the monomers with respect to each other. Minimization was

carried out in 100 steps with the use of the repel function in X-PLOR 3.1 (Powell minimization option). In the analysis, the Van der Waals energy was calculated between the monomer subunits only.

Acknowledgements

[1] C. C. Moser, P. L. Dutton, *Protein Electron Transfer* (Ed.: D. S. Bendall), Bios Scientific Publishers, Oxford, UK, **1996**, pp. 1–21.
[2] R. A. Marcus, N. Sutin, *Biochim. Biophys. Acta* **1985**, *811*, 265–322.
[3] T. A. Alleyne, M. T. Wilson, G. Antonini, F. Malatesta, B. Vallone, P. Sarti, M. Brunori, *Biochem. J.* **1992**, *287*, 951–956.
[4] C. Correia, E. Monzani, I. Moura, J. Lampreia, J. J. G. Moura, *Biochem. Biophys. Res. Commun.* **1999**, *256*, 367–371.
[5] J. L. Dickerson, J. J. Kornuc, D. C. Rees, *J. Biol. Chem.* **1985**, *260*, 5175–5178.
[6] J. E. Erman, K. L. Kim, L. B. Vitello, S. J. Moench, J. D. Satterlee, *Biochim. Biophys. Acta* **1987**, *911*, 1–10.
[7] J. T. Hazzard, S. J. Moench, J. E. Erman, J. D. Satterlee, G. Tollin, *Biochemistry* **1988**, *27*, 2002–2008.
[8] F. Malatesta, G. Antonini, F. Nicoletti, A. Giuffrè, E. D'Itri, P. Sarti, M. Brunori, *Biochem. J.* **1996**, *315*, 909–916.
[9] S. J. Moench, J. D. Satterlee, J. E. Erman, *Biochemistry* **1987**, *26*, 3821–3826.
[10] S. J. Moench, J. E. Erman, J. D. Satterlee, *Int. J. Biochem.* **1993**, *25*, 1335–1342.
[11] U. Mühlenhoff, J. Zhao, D. A. Bryant, *Eur. J. Biochem.* **1996**, *235*, 324–331.
[12] L. M. Peerey, N. M. Kostić, *Biochemistry* **1989**, *28*, 1861–1868.
[13] L. M. Peerey, H. M. Brothers, J. T. Hazzard, G. Tollin, N. M. Kostiæ, *Biochemistry* **1991**, *30*, 9297–9304.
[14] L. Qin, N. M. Kostić, *Biochemistry* **1993**, *32*, 6073–6080.
[15] J. S. Zhou, H. M. Brothers, J. P. Neddersen, L. M. Peerey, T. M. Cotton, N. M. Kostić, *Bioconjug. Chem.* **1992**, *3*, 382–390.
[16] J. S. Zhou, N. M. Kostić, *Biochemistry* **1992**, *31*, 7543–7550.
[17] H. S. Pappa, T. L. Poulos, *Biochemistry* **1995**, *34*, 6573–6580.
[18] H. S. Pappa, S. Tajbaksh, A. J. Saunders, G. J. Pielak, T. L. Poulos, *Biochemistry* **1996**, *35*, 4837–4845.
[19] M. M. Crnogorac, C. Shen, S. Young, Ö. Hansson, N. M. Kostić, *Biochemistry* **1996**, *35*, 16465–16474.
[20] M. Hervás, J. A. Navarro, A. Díaz, H. Bottin, M. A. De la Rosa, *Biochemistry* **1995**, *34*, 11321–11326.
[21] M. M. Ivković-Jensen, G. M. Ullmann, S. Young, Ö. Hansson, M. M. Crnogorac, M. Ejdebäck, N. M. Kostić, *Biochemistry* **1998**, *37*, 9557–9569.
[22] M. Ubbink, M. Ejdebäck, B. G. Karlsson, D. S. Bendall, *Structure* **1998**, *6*, 323–335.
[23] G. M. Ullmann, E. W. Knapp, N. M. Kostić, *J. Am. Chem. Soc.* **1997**, *119*, 42–52.
[24] E. T. Adman, *Adv. Protein Chem.* **1991**, *42*, 145–197.
[25] G. W. Canters, G. Gilardi, *FEBS Lett.* **1993**, *325*, 39–48.
[26] H. Nar, A. Messerschmidt, R. Huber, M. van de Kamp, G. W. Canters, *J. Mol. Biol.* **1991**, *221*, 765–772.
[27] H. Nar, A. Messerschmidt, R. Huber, M. van de Kamp, G. W. Canters, *J. Mol. Biol.* **1991**, *218*, 427–447.
[28] A. G. Sykes, *Adv. Inorg. Chem.* **1991**, *36*, 377–408.
[29] M. van de Kamp, M. C. Silvestrini, M. Brunori, J. Van Beeumen, F. C. Hali, G. W. Canters, *Eur. J. Biochem.* **1990**, *194*, 109–118.
[30] A. P. Kalverda, M. Ubbink, G. Gilardi, S. S. Wijmenga, A. Crawford, L. J. C. Jeuken, G. W. Canters, *Biochemistry* **1999**, *38*, 12690–12697.
[31] A. P. Kalverda, M. Ubbink, G. Gilardi, S. S. Wijmenga, A. Crawford, L. J. C. Jeuken, G. W. Canters, *Biochemistry* **1999**, *38*, 12690–12697.
[32] G. van Pouderoyen, S. Mazumdar, N. I. Hunt, H. A. O. Hill, G. W. Canters, *Eur. J. Biochem.* **1994**, *222*, 583–588.
[33] M. van de Kamp, R. Floris, F. C. Hali, G. W. Canters, *J. Am. Chem. Soc.* **1990**, *112*, 907–908.
[34] M. van de Kamp, G. W. Canters, C. R. Andrew, J. Sanders-Loehr, C. J. Bender, J. Peisach, *Eur. J. Biochem.* **1993**, *218*, 229–238.
[35] G. W. Canters, H. A. O. Hill, N. A. Kitchen, E. T. Adman, *J. Magn. Reson.* **1984**, *57*, 1–23.
[36] C. M. Groeneveld, G. W. Canters, *Eur. J. Biochem.* **1985**, *153*, 559–564.
[37] C. M. Groeneveld, G. W. Canters, *J. Biol. Chem.* **1988**, *263*, 167–173.
[38] K. V. Mikkelsen, L. K. Skov, H. Nar, O. Farver, *Proc. Natl. Acad. Sci. USA* **1993**, *90*, 5443–5445.
[39] P. W. Riddles, R. L. Blakeley, B. Zerner, *Methods Enzymol.* **1983**, *91*, 49–60.
[40] M. Ubbink, L. Y. Lian, S. Modi, P. A. Evans, D. S. Bendall, *Eur. J. Biochem.* **1996**, *242*, 132–147.
[41] A. T. Brunger, X-PLOR 3.1 manual, Yale University Press, New Haven, CT, USA, **1993**.
[42] C. C. Moser, P. L. Dutton, *Biochim. Biophys. Acta* **1992**, *1101*, 171–176.
[43] O. Farver, L. K. Skov, G. Gilardi, G. van Pouderoyen, G. W. Canters, S. Wherland, I. Pecht, *Chem. Phys.* **1996**, *204*, 271–277.
[44] H. B. Gray, B. G. Malmström, R. J. P. Williams, *J. Biol. Inorg. Chem.* **2000**, *5*, 551–559.
[45] J. Navaza, *Acta Crystallogr. Sect. A* **1994**, *50*, 157–163.
[46] V. Picard, E. Ersdal-Badju, A. Lu, S. C. Bock, *Nucleic Acids Res.* **1994**, *22*, 2587–2591.
[47] M. van de Kamp, F. C. Hali, N. Rosato, A. Finazzi Agro, G. W. Canters, *Biochim. Biophys. Acta* **1990**, *1019*, 283–292.
[48] H. Nar, R. Huber, A. Messerschmidt, A. C. Filippou, M. Barth, M. Jaquinod, M. van de Kamp, G. W. Canters, *Eur. J. Biochem.* **1992**, *205*, 1123–1129.
[49] P. J. Kraulis, *J. Appl. Crystallogr.* **1991**, *24*, 946–950.